CORA Cork Open Research Archive
Cartlann Taighde Oscailte Chorcaí

| | |
|---|---|
| Title | Role of surface reconstruction on Cu/TiO2 nanotubes for CO2 conversion |
| Authors | Liu, Chao;Nauert, Scott L.;Alsina, Marco A.;Wang, Dingdi;Grant, Alexander;He, Kai;Weitz, Eric;Nolan, Michael;Gray, Kimberly A.;Notestein, Justin M. |
| Publication date | 2019-05-16 |
| Original Citation | Liu, C., Nauert, S. L., Alsina, M. A., Wang, D., Grant, A., He, K., Weitz, E., Nolan, M., Gray, K. A. and Notestein, J. M. (2019) 'Role of surface reconstruction on Cu/TiO2 nanotubes for CO2 conversion', Applied Catalysis B: Environmental, 255, 117754 (9 pp). doi: 10.1016/j.apcatb.2019.117754 |
| Type of publication | Article (peer-reviewed) |
| Link to publisher's version | http://www.sciencedirect.com/science/article/pii/S092633731930493X - 10.1016/j.apcatb.2019.117754 |
| Rights | © 2019 Elsevier B.V. All rights reserved. This manuscript version is made available under the CC-BY-NC-ND 4.0 license - http://creativecommons.org/licenses/by-nc-nd/4.0/ |
| Download date | 2026-10-05 12:43:59 |
| Item downloaded from | https://hdl.handle.net/10468/8340 |

UCC
University College Cork, Ireland
Coláiste na hOllscoile Corcaigh

*Revised Manuscript
Click here to view linked References

# Role of surface reconstruction on $Cu/TiO_2$ nanotubes for $CO_2$ conversion

Chao Liu,[1] Scott L. Nauert,[2] Marco A. Alsina,[1] Dingdi Wang,[3] Alexander Grant,[2] Kai He,[4] Eric Weitz,[3,*] Michael Nolan,[5] Kimberly A. Gray,[1,*] Justin M. Notestein[2,*]

[1]Department of Civil and Environmental Engineering, [2]Department of Chemical and Biological Engineering, [3]Department of Chemistry, [4]Department of Materials Science and Engineering, Northwestern University, Evanston, Illinois 60208, United States
[5]Tyndall National Institute, University College Cork, Lee Maltings, Cork, Ireland

## Abstract

Carbon dioxide hydrogenation to CO via the reverse water gas shift (RWGS) reaction is one route to integrate $CO_2$ utilization into the chemical industry. $TiO_2$ supported Cu catalysts are known to be active for RWGS, but Cu is shown here to behave differently on $TiO_2$ nanotubes (TiNT) vs $TiO_2$ nanoparticles (TiNP). Whereas nanoparticle supports give low rates that are hardly changed by added Cu, the nanotube supports yield much higher activity and three distinct behaviors as the Cu surface density increases. At low surface densities (0.3 $Cu/nm^2$), active Cu-O-Ti sites are created that have low apparent activation energies. At high surface densities (6 $Cu/nm^2$), Cu nanoparticles on TiNT are formed, and reaction barriers are lowered when both Cu and TiNT surfaces are accessible. At intermediate surface densities, metallic Cu domains are engulfed by a TiOx overlayer formed during $H_2$ pretreatment, akin to those formed by classical strong metal support interactions (SMSI). These reduced layers are markedly more active for RWGS than the initial TiNT surfaces, but have similar activation barriers, which are higher than those for which both Cu and TiNP surfaces are exposed. These catalytic findings are supported by computational modeling, *in situ* IR, UV-visible, and X-ray absorption spectroscopies, and they provide insight into an important reaction for $CO_2$ utilization.

## Keywords

reverse water-gas shift; SMSI; supported metals; carbon; spectroscopy

## Introduction

Conversion of $CO_2$ to feedstock chemicals is a key step in remaking the value chain and creating carbon neutral cycles in the chemical industry[1,2] The water gas shift and reverse water gas shift (RWGS) reactions ($CO + H_2O \leftrightarrow CO_2 + H_2$) are well-known and widely utilized in industry to adjust the ratios of CO and $H_2$ in syngas for the Fischer-Tropsch process[3,4]. RWGS is endothermic and thermodynamically favored at elevated temperature[5], making it an inevitable reaction during any $CO_2$ hydrogenation process. For example, Rodriguez et al. found that RWGS and methanol synthesis have similar apparent activation energies on a Cu/CeOx catalyst[6].

Cu catalysts are considered as among the more promising catalysts for RWGS since CO, the product, does not interact strongly with metallic Cu[7]. $TiO_2$ supported Cu catalysts have been reported to catalyze the conversion of $CO_2$ to CO, methane and methanol[8-11]. A potential complicating factor in understanding these materials is the requirement to activate the catalysts in $H_2$ to form metallic or low oxidation state Cu species[12-23], create oxygen vacancies or undercoordinated Ti sites on $TiO_2$[22,23], and to remove carbonaceous species[15]. Although metal nanoparticles on $TiO_2$ and other reducible supports are well known to reconstruct in reducing environments[24-26], the potential role of the surface reconstruction of Cu/$TiO_2$ catalysts in $CO_2$ conversion reactions is not well understood.

$TiO_2$ nanotubes (TiNT), with their unique morphology[27,28], have been shown to preferentially adsorb and activate $CO_2$ with the aid of photo-induced electrons[29,30]. In initiating this study, we hypothesized that using TiNT as supports for copper would result in improved behavior in RWGS, as compared to Cu supported on conventional $TiO_2$ nanopowder (TiNP) In testing this hypothesis, we indeed observed increased activity, but we also observed a complex dependence of the rate on the Cu surface density on the TiNT support that demanded further investigation.

Our analysis with *in situ* IR, UV-vis, and X-ray absorption spectroscopies together with DFT calculations lead to the conclusion that surface reconstruction is responsible for the pattern of activity of these materials.

## Experimental

$TiO_2$ nanotubes (TiNT) were prepared by reconstructing anatase $TiO_2$ (Sigma, 99.7%, <25 nm particle size) using a hydrothermal method[31]. The TiNT materials were calcined in a flow of air at 450 °C for 5 hours. Cu/TiNP and Cu/TiNT were prepared by incipient wetness impregnation of $Cu(NO_3)_2 \cdot 3H_2O$ (Sigma, 99.999%) on $TiO_2$ nanopowder (TiNP) and TiNT following a previously described procedure[32], and finally calcined in a flow of air at 450 °C for 4 hours. This latter step is expected to collapse the nanotubes somewhat[31], reducing surface areas while retaining the surface termination. The Cu catalysts were prepared with nominal surface densities of 0.3 Cu/nm$^2$, 1.5 Cu/nm$^2$, 3 Cu/nm$^2$ and 6 Cu/nm$^2$. The latter is denoted, for example, 6Cu/TiNT. Measured Cu loadings and other physical properties are given in **Table 1**.

Nitrogen adsorption-desorption isotherms were collected using a Micromeritics ASAP 2010 instrument. The elemental compositions of Cu and Ti were determined by a Thermo iCAP 7600 ICP-OES. Raman spectra were collected using a HORIBA LabRAM HR Evolution Confocal Raman with a 785 nm excitation laser. X-ray diffraction (XRD) data were collected using a Rigaku Ultima X-ray diffractometer. Temperature Programmed Reduction (TPR) data were collected using 10% $H_2/N_2$ as the reductant in an Altamira AMI-200 reactor system over a temperature range of 40 – 340 °C. *In situ* DRIFTS experiments averaged 64 scans at 4 cm$^{-1}$ resolution from a Nicolet 6700 FTIR spectrometer equipped with a Harrick Praying Mantis diffuse reflectance accessory and an MCT detector.

*In situ* UV-visible spectra were collected with a Shimadzu UV-3600 spectrometer equipped with a Harrick Praying Mantis diffuse reflectance accessory. The Harrick cell was slightly modified by putting the tip of a thermocouple just under the sample surface, and close to the spot at which spectra were recorded, in order to accurately measure the surface temperature. Barium sulfate (Sigma, 99.998%) was used as the baseline reference for all samples. The sample in the cell was pretreated at 300 °C in Ar for 30 minutes before any further treatment. *In situ* experiments were performed using $H_2$ (Airgas, 99.999%) and $CO_2$ (Airgas, 99.999%) at a flow rate of 20 ml/min at 300 °C.

High-resolution transmission electron micrographs were obtained on a JEOL 2100F TEM operating at 200 kV. The samples were dispersed in ethanol and drop-casted on a holey carbon-coated Cu grid for imaging.

Periodic plane wave DFT calculations were carried out on anatase $TiO_2$ modified with Cu as a model for the 0.3 Cu-TiNT system. These were performed using the VASP5.2 code[33,34] with a kinetic energy cut-off of 400 eV. The core-valence interaction was described using the projector augmented wave (PAW) potentials[35,36], with 4 valence electrons for Ti, 6 for O and 11 for Cu. The Perdew-Wang (PW91) approximation to the exchange-correlation functional was used[37]. The $TiO_2$ anatase (001) substrate was modelled as an 18 atomic layer slab, with a $(4\times 4)$ surface supercell expansion ($a$ = 15.324 Å, $b$ = 15.329 Å) and a vacuum gap of 12 Å. This surface was chosen since the anatase (001) facet is characteristic of TiNT and partially collapsed TiNT[27]. Due to the surface supercell expansion used, Γ-point sampling was used and the convergence criteria for the energy and forces were $10^{-4}$ eV and $0.02$ eV.$Å^{-2}$, respectively. All calculations were spin polarized and there were no symmetry restraints applied. Hubbard U corrections were implemented, with U(Ti) = 4.5 eV and U(Cu) = 7 eV, to consistently describe

the partially filled Cu 3d states, particularly where $Cu^{2+}$ and reduced $Ti^{3+}$ cations are possible[38,39]. Cation oxidation states were determined from Bader charge analysis and spin mangetisations. To model the different surface modifications, we considered the adsorption and relaxation of a Cu atom and a CuO moiety on anatase (001) and the impact on reducibility and $CO_2$ adsorption. To this end, different adsorption sites for Cu and CuO were examined and the most stable are shown in the Results and Discussion section.

Catalytic measurements were conducted in a packed-bed tubular stainless-steel reactor (0.25 inch diameter) using 0.1 g catalyst mixed with 0.1 g quartz sand with the same particle size. The catalysts were crushed to particles below 105 microns in order to avoid intraparticle mass transfer limitations. The feed gas mixtures of $CO_2$ (Airgas, 99.999%), $H_2$ (Airgas, 99.999%) and He (Airgas, 99.999%) were supplied by mass flow controllers. In each experiment, the catalyst in the reactor was reduced in $H_2$ at 340 °C for 2 hours prior to reacting with 3 MPa of mixtures of $CO_2$ and $H_2$ for 3 hours at temperatures of 200 °C, 235 °C, 270 °C, 305 °C and 340 °C. Each Cu/TiNP catalyst was tested twice, and each Cu/TiNT catalyst was tested three times. The products were monitored with an online Shimadzu GC-2010, equipped with a Rt-U-BOND column, a Rt-sieve 5A PLOT column, and a TCD detector. CO was the only detected product in all cases. Conversions are kept to <10% of equilibrium yield for all trials to ensure differential conversion and to minimize the need to correct rates for the approach to equilibrium.

**Results and Discussion**

RWGS kinetics were examined in a flow reactor, and CO production rates over the various catalysts are compared in **Figure 1**. Figure 1 only shows a single loading for Cu/TiNP because loading did not have a significant impact on either CO generation rates (30-65 μmol CO $g_{cat}^{-1}$ $min^{-1}$ at 340 ºC) or the apparent activation energies (~100 kJ/mol; Figure S1 and Table S1).

However, for Cu/TiNT, the CO production rates were much higher than those over Cu/TiNP and depended significantly on the loading of Cu (50-900 μmol CO $g_{cat}^{-1}$ $min^{-1}$ at 340 ºC) when going from ~5% of a monolayer (0.3 Cu/$nm^2$) to approximately monolayer loading (6 Cu/$nm^2$). Rates normalized per total Cu loading are given in Figure S2, where 0.3Cu/TiNT shows slightly higher activity than the other Cu/TiNT catalysts, which are similar to each other. Because TiNT has non-negligible activity of its own (Figure 1) and because the nature of the active site is not immediately known, the discussion is based on rates per gram of total catalyst. The data in Figure 1 also reveal catalysts with three distinct apparent activation energies (**Table 1**). Catalysts TiNT, 1.5Cu/TiNT, and 3Cu/TiNT have barriers of ~102 kJ/mol, while that of 6Cu/TiNT is only 81 kJ/mol. The apparent barrier for 0.3 Cu/TiNT is lower still at 65 kJ/mol.

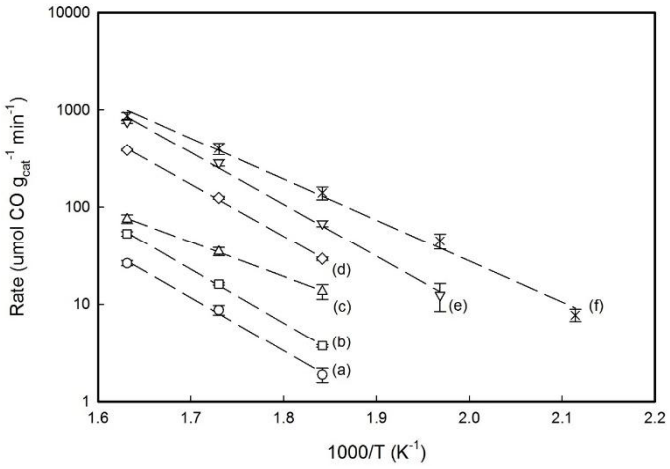


**Figure 1.** Arrhenius plots for the reverse water gas shift over (a) 1.5Cu/TiNP as a representative nanoparticle (TiNP) supported catalyst, (b) TiNT, (c) 0.3Cu/TiNT, (d) 1.5Cu/TiNT, (e) 3Cu/TiNT, and (f) 6Cu/TiNT. Reaction conditions: 3 MPa, $H_2/CO_2$ = 1/1 (v/v), WHSV = 36000 ml $g_{cat.}^{-1}h^{-1}$

**Table 1.** Cu/TiNT properties and catalytic performance

| Material[a] | Surface Area ($m^2/g$) | Pore Volume ($cm^3/g$) | Cu Loading (wt%) | Surface Density ($Cu/nm^2$) | Apparent Activation Energy[b] (kJ/mol) |
|---|---|---|---|---|---|
| TiNT | 155 | 0.57 | - | - | 105 |
| 0.3Cu/TiNT | 119 | 0.53 | 0.4 | 0.2 | 65 |
| 1.5Cu/TiNT | 110 | 0.51 | 2.7 | 1.7 | 102 |
| 3Cu/TiNT | 101 | 0.50 | 4.5 | 2.8 | 98 |
| 6Cu/TiNT | 94 | 0.44 | 9.1 | 5.6 | 81 |

[a] See supporting information Figure S1 and Table S1 for physical properties and apparent barriers over TiNP-based materials.
[b] From the slopes of Figure 1. Values ± 5 kJ/mol

Raman spectra of the as-prepared Cu/TiNT materials are shown in Figure S3. Antase[40] $TiO_2$ is present in all samples as expected, and crystalline CuO[41] is observed in the 1.5Cu/TiNT, 3Cu/TiNT and 6Cu/TiNT samples.

Normalized TPR profiles of the as-synthesized Cu/TiNT catalysts are plotted from 40 °C to 340 °C in **Figure 2**, and the first reduction peak decreased in temperature as the Cu loading increased from 1.5 $Cu/nm^2$ to 6 $Cu/nm^2$ (Figures 2b – 2d, marked by red arrows). A similar trend has been reported by other researchers[42], and is attributed to the decrease in the portion of strongly-coordinated Cu on $TiO_2$ as CuO dispersion decreases. Most of the reduction occurred in a characteristic two-step fashion between 160 - 300 °C, where crystalline CuO supported on $TiO_2$ typically reduces[42-45]. 0.3 Cu/TiNT is an outlier for this trend, with a relatively low-temperature reduction event. We recently studied very highly dispersed, non-crystalline CuO, such as found in the 0.3 Cu/TiNT (~5% of a monolayer) sample, and observed that the samples became more reducible as loading decreased.[46] This was ascribed to Cu sites being located in highly reactive defects found in very small amounts on support surfaces.

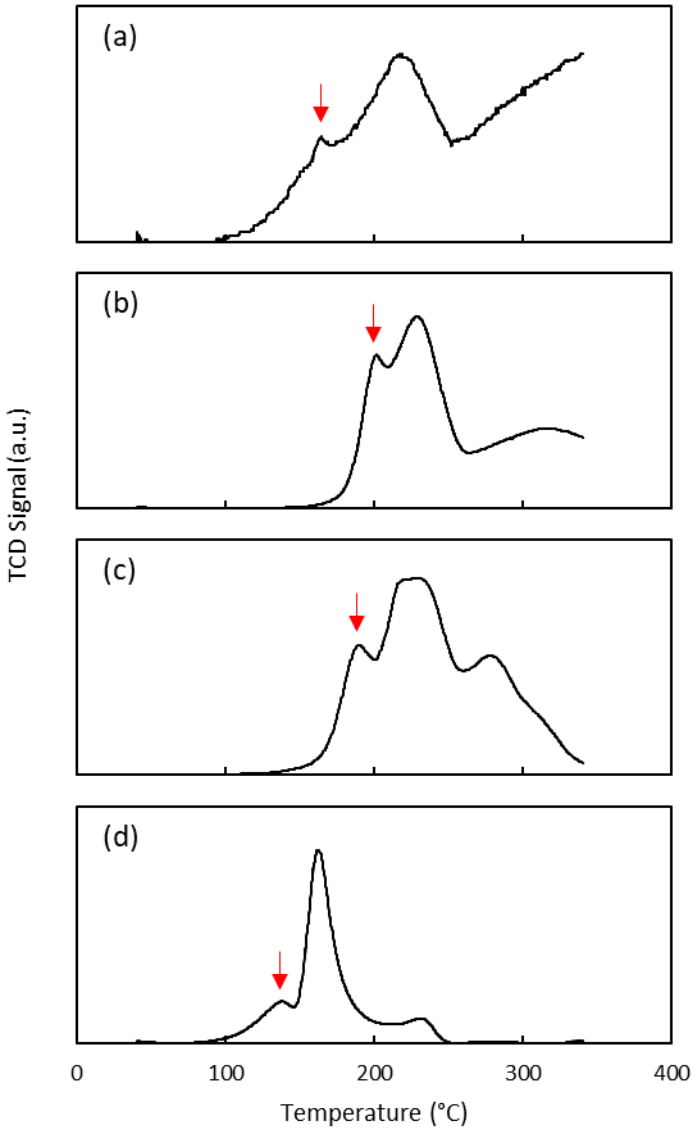


**Figure 2**. $H_2$-TPR profiles of (a) 0.3Cu/TiNT, (b) 1.5Cu/TiNT, (c) 3Cu/TiNT, and (d) 6Cu/TiNT. Signals are nomalized to the maximum intensity feature. Arrows mark the first reduction event. $H_2$ consumption above 300°C in (a) arises from the TiNT support itself and becomes proportionally less significant with increasing Cu loading.

Because of its easy reducibility and low apparent barrier to $CO_2$ hydrogenation, the structure and reducibility of the species likely present on the surface of the 0.3Cu/TiNT sample were examined in detail with first principles density functional theory simulations. **Figure 3a** shows a model structure for this low Cu coverage material, which is composed of an isolated CuO species adsorbed on the anatase (001) surface, the highest energy surface of $TiO_2$ and the preferred

orientation in TiNT [27]. This 0.3Cu/TiNT surface has exclusively $Cu^{2+}$ and $Ti^{4+}$ surface species. Removal of an O atom from the structure in Figure 3a, to simulate autothermal reduction, requires 1.94 eV, and it produces $Ti^{3+}$ and $Cu^{+}$ in a typical O-Cu-O dumbbell structure (Figures 3b and 3c). In contrast, the removal of an O atom to form two $Ti^{3+}$ cations and a $Cu^{2+}$ cation is less stable. In turn, these energies are much lower than the calculated cost of 3.37 eV to remove an O atom from the unmodified anatase (001) surface and generate two $Ti^{3+}$ species within the same computational geometry. Hydrogenation of the surface to give a surface-bound $H_2O$ is significantly exothermic by 1.84 eV (Figures 3d and 3e), but as before, this gives a $Ti^{3+}$ and $Cu^{+}$ in a similar structure. See Figure S4 and accompanying text for further details of these calculations. Thus, reduction of CuO-modified anatase (001) is more favourable than the bare anatase (001) and in addition always produces a $Cu^{+}$ and a $Ti^{3+}$ cation, rather than only activating nearby Ti-O-Ti sites. These $Cu^{+}/Ti^{3+}$ sites resulting from $H_2$ reduction are then models of potential sites for $CO_2$ adsorption and activation at Ti-O-Cu interfaces.

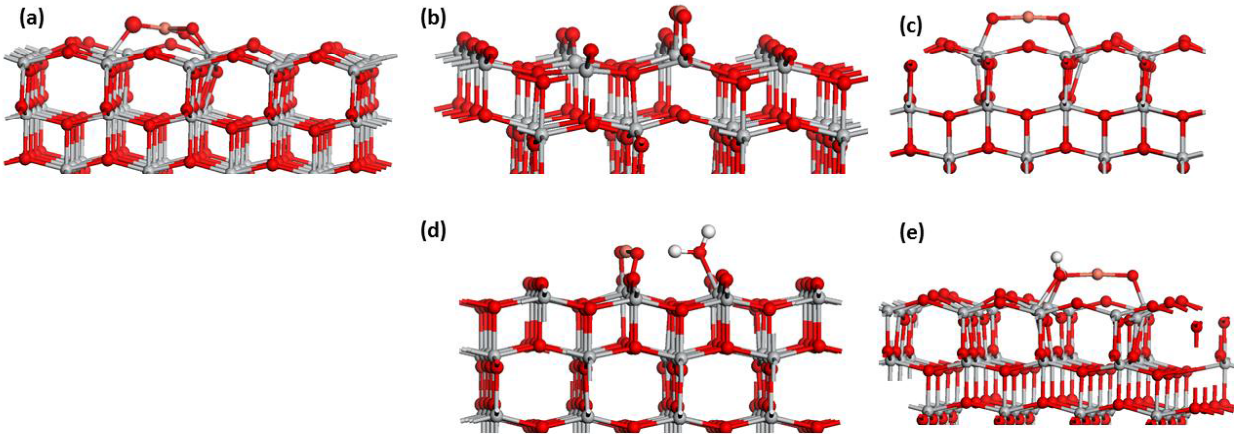


**Figure 3. (a)** Atomic structure of a CuO species modifying anatase (001) **(b)** and **(c):** atomic structure of CuO-modified anatase (001) after removal of the most stable reducing oxygen vacancy. **(d)** and **(e):** atomic structure of CuO-modified anatase (001) after formation of water by $H_2$ adsorption. **(b)/(c)** and **(d)/(e)** show two views of each structure. In this and all figures, Ti is represented by grey spheres, oxygen by red spheres, Cu by brown spheres and H by white spheres.

*In situ* diffuse reflectance UV-visible spectroscopy provides additional information about the speciation of Cu on the surface under reducing pretreatments and with exposure to reactants. In the top panels of **Figure 4**, the as-synthesized catalysts were heated to 300 °C under continuous flow of Ar, and the initial spectra were acquired. The gas was switched to $H_2$ (20 ml/min), and their absorption edges red shifted over 10 minutes due to the reduction of Cu and the TiNT support[47, 48]. The characteristic absorption band for metallic Cu nanoparticles, at around 600 nm[49], is discernible for the 1.5Cu/TiNT, 3Cu/TiNT and 6Cu/TiNT samples, but is not for 0.3Cu/TiNT. The assignment of metallic nanoparticles of Cu on these three surfaces is also supported by *ex situ* XRD patterns of the freshly reduced materials (Figure S5) and by TEM of the reduced surfaces (Figure S6). No nanoparticles or crystalline Cu were discernable on the 0.3 Cu/TiNT sample. When the $H_2$-treated materials were subsequently purged in He and then exposed to $CO_2$ (20 mL/min) at 300 °C, the absorption bands of the lowest and highest-loaded samples, 0.3Cu/TiNT and 6Cu/TiNT, were blue shifted back to their original state within 5 minutes, indicating the re-oxidation of Cu by $CO_2$. In contrast, the absorption bands from metallic Cu on the reduced 1.5Cu/TiNT and 3Cu/TiNT samples were much less changed, even after 30 minutes exposure to $CO_2$ at 300 °C. At 300 °C and atmospheric pressure, $CO_2$ is known to dissociatively adsorb on - and consequently oxidize - metallic Cu surfaces[50-52]. Therefore, the re-oxidation of Cu on 0.3Cu/TiNT and 6Cu/TiNT indicates Cu atoms accessible to $CO_2$, whereas the persistence of metallic Cu in 1.5Cu/TiNT and 3Cu/TiNT indicates the Cu on those samples is inaccessible to $CO_2$.

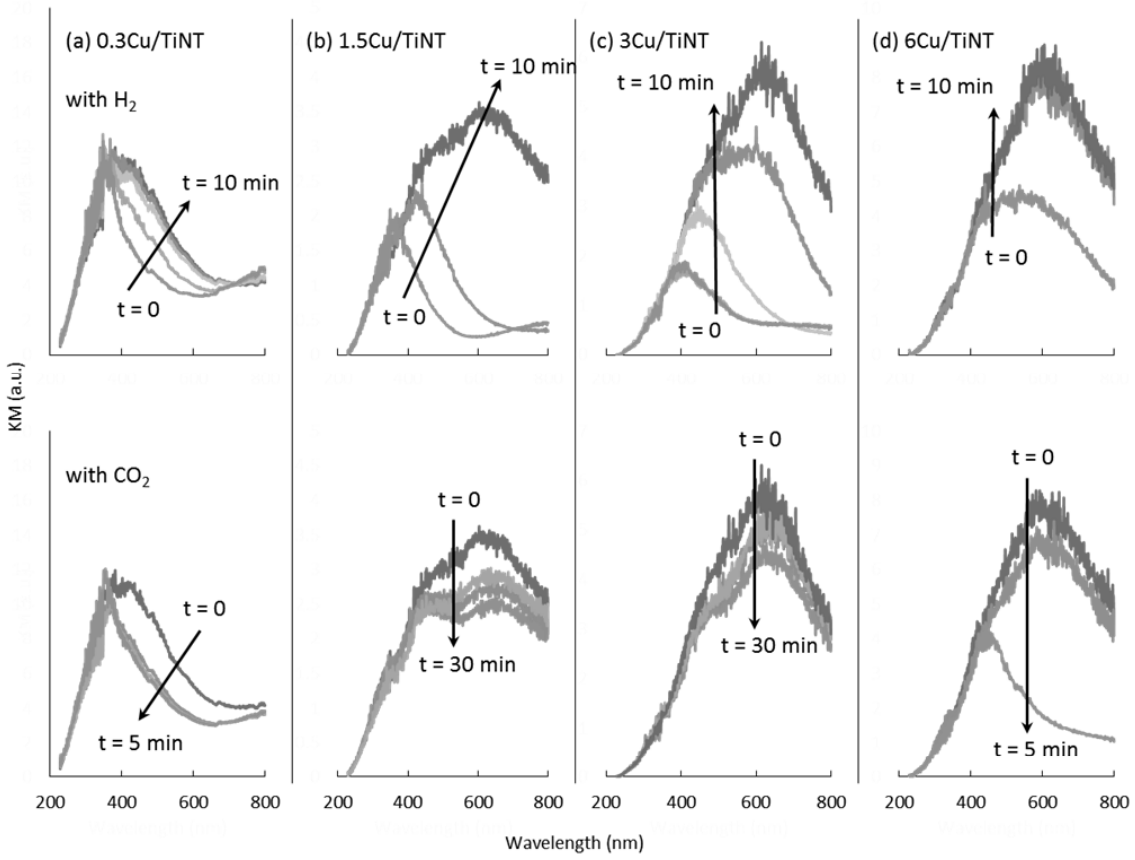


**Figure 4.** *In situ* UV-Vis spectra of (a) 0.3Cu/TiNT, (b) 1.5Cu/TiNT, (c) 3Cu/TiNT and (d) 6Cu/TiNT at 300 °C. The arrows indicate the increase in time under a continuous flow of $H_2$ (top panels) and, subsequently, $CO_2$ (bottom panels)

The vibrational modes of surface carbonates derived from $CO_2$ chemisorption were next used to probe the TiNT surfaces. Similar to the *in situ* UV-visible studies, the samples were heated to 300 °C under a continuous flow of Ar, reduced in $H_2$ at 300 °C for 30 minutes, purged in Ar for 60 minutes, and background spectra were collected. $CO_2$ was allowed to flow over the samples for 15 minutes and the gas was then switched back to Ar to purge the cell of gaseous $CO_2$. **Figure 5** shows the spectra recorded at 5 minutes after the gas flow was switched back to Ar. The spectrum obtained on adsorption of $CO_2$ on $TiO_2$ nanoparticles (TiNP) is shown in Figure 5a, where the absorption at 1225 $cm^{-1}$ is attributed to bicarbonate[53], and 1658 $cm^{-1}$ is assigned to the bending mode of water. Both bidentate (1318 $cm^{-1}$) and monodentate carbonate (1447 and

1379 $cm^{-1}$) species are observed on TiNP. As a result, $CO_2$ adsorbed on TiNP has strong IR absorption from 1800 to 1500 $cm^{-1}$, owing to the convoluted spectra of bidentate and monodentate carbonate species. However, the spectrum of $CO_2$ adsorbed on TiNT (Figure 5b) is dominated by features assigned to water (1616 $cm^{-1}$)[54,55] and monodenteate carbonate (1521, 1426, and 1374 $cm^{-1}$)[56].

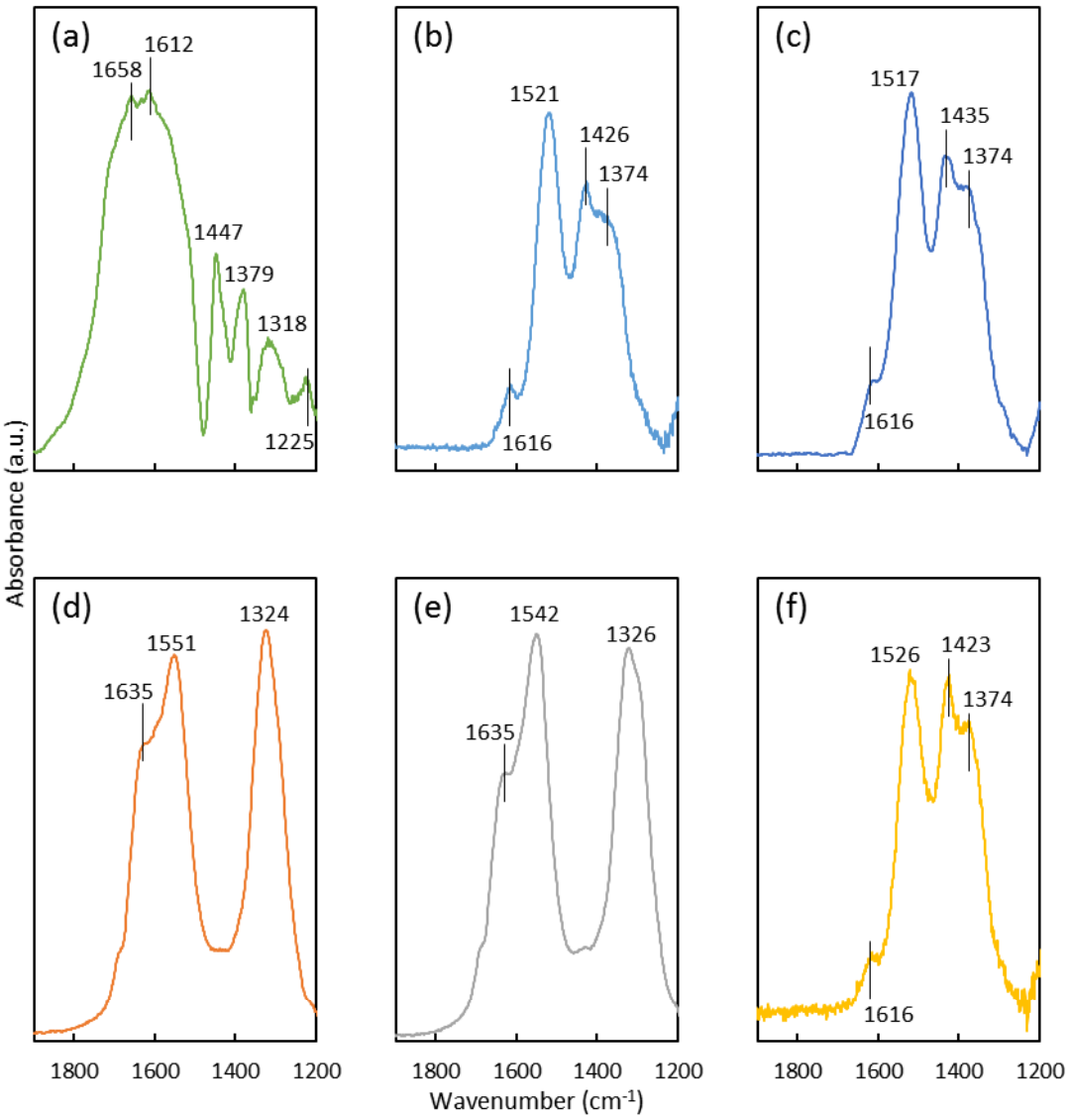


**Figure 5.** IR spectra of $CO_2$ adsorption on the reduced surfaces of (a) $TiO_2$ nanoparticles (TiNP), (b) TiNT, (c) 0.3Cu/TiNT, (d) 1.5Cu/TiNT, (e) 3Cu/TiNT, and (f) 6Cu/TiNT. Samples were heated to 300 °C under flowing Ar, then $H_2$, then $CO_2$. See main text for full experimental conditions.

The spectrum of 0.3Cu/TiNT (Figure 5c) does not differ significantly from that of TiNT, as expected from the low amounts of Cu present, but one monodentate carbonate peak is red-shifted from 1521 $cm^{-1}$ on TiNT to 1517 $cm^{-1}$ on 0.3Cu/TiNT and another blue shifts from 1426 $cm^{-1}$ on TiNT to 1435 $cm^{-1}$. These shifts suggest that the monodentate carbonate species were adsorbed on Cu-O-Ti sites of 0.3Cu/TiNT and on Ti-O-Ti sites of TiNT.

Three strong, well-resolved absorption bands at 1635, 1551 (1542), and 1324 (1326) $cm^{-1}$, are seen with the 1.5Cu/TiNT and 3Cu/TiNT samples (Figures 5d and 5e), The absorption at 1635 $cm^{-1}$ is assigned to the bending mode of surface water and is blue-shifted relative to that on 0.3Cu/TiNT or TiNT. This shift is usually attributed to an increase in the concentration of water[57,58]. The latter two bands were identified in our previous study[29] as a bidentate carbonate on $TiO_2$. For the highest loaded 6Cu/TiNT (Figure 5f), the IR spectrum more strongly resembles that of low-loading 0.3Cu/TiNT than it does the intermediate loading samples, and the features at 1526 $cm^{-1}$ and 1423 $cm^{-1}$ are analogously assigned as monodentate carbonates.

We have also investigated $CO_2$ adsorption on the reduced surfaces of our computational model of 0.3Cu/TiNT, which shows a number of possible interactions that are consistent with this vibrational spectrum, but which depend on the nature of the oxygen vacancy initially formed. There are three different favorable interaction configurations of $CO_2$ with reduced 0.3Cu/TiNT, with computed $CO_2$ adsorption energies of -0.25 eV, -1.04 eV, and -2.50 eV. The two strongest adsorption modes shown in **Figure 6**. Here, the $CO_2$ adsorbs in an activated form, where C-O bonds elongate and form carbonate-like structures. In all the adsorption geometries, at least one C-O bond forms between the Cu and Ti atoms, again highlighting the key role of the Cu-O-Ti interface at this low coverage of Cu. No significant charge is transferred between the Cu and Ti

surface atoms and the $CO_2$, consistent with initial formation of a carbonate and indicating that the initial reduction of C and re-oxidation of Cu/Ti does not occur spontaneously. This is expected from the overall endothermicity of the RWGS reaction. A more detailed discussion of adsorption geometries is given in Figure S7 and accompanying text. While we observe that the strength of the interaction with $CO_2$ and that the final structure of the complex between Cu and adsorbed $CO_2$ depend on which O atom is removed during the initial reduction step, a critical result is that $CO_2$ adsorption is always preferentially found at the Cu-O-Ti interface. Further studies should addres the role of exposed Cu in larger nanoparticles.

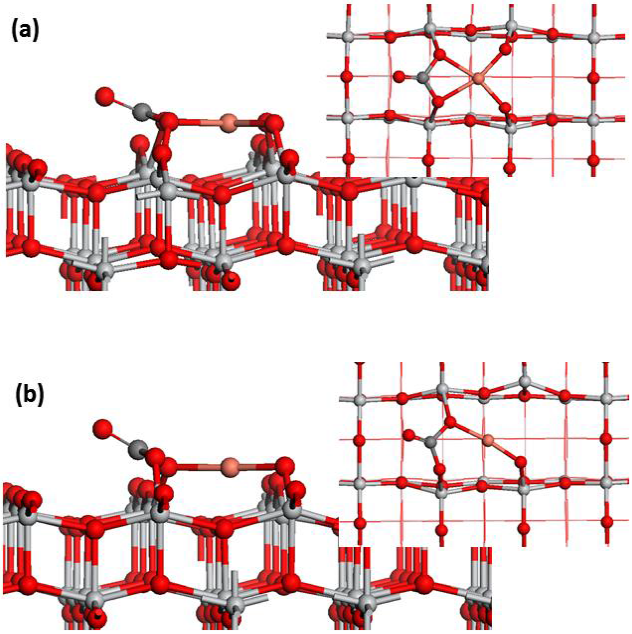


**Figure 6.** Side and top views of two possible carbonate-like adsorption modes of $CO_2$ with models of the reduced surface of 0.3Cu/TiNT (from Figure 3c). Colour coding is the same as Figure 3, with carbon shown by the grey sphere.

We explain the different $CO_2$ adsorption features on the high/low vs. intermediate loadings of Cu/TiNT catalysts by surface reconstructions akin to a strong metal support interaction (SMSI)[59]. In reducing atmospheres around or above 300 °C, $TiO_2$ supports are well known to form a non-crystalline, reduced form of SMSI overlayers on supported metals[26,60]. As

illustrated in **Scheme 1**, we propose that SMSI overlayers on 1.5Cu/TiNT and 3Cu/TiNT totally encapsulate the Cu nanoparticle surface after pretreatment in $H_2$. This prevents the re-oxidation of Cu by $CO_2$ in the *in situ* UV-visible experiments, and leads to the surface being dominated by a reconstructed TiOx surface distinct from that found on the original TiNT, explaining the changes in the IR spectra. Highly reactive defect sites (e.g. O vacancies) will be more numerous on the SMSI surface than on the bare TiNT surface, explaining the increase in rate absent a change in activation barrier. In contrast, SMSI overlayers do not appear to have completely engulfed the Cu nanoparticles in 6Cu/TiNT, and the exposed interfaces allow the Cu nanoparticles and TiOx SMSI to re-oxidize during *in situ* UV-visible spectroscopy. The inability to form a complete SMSI layer is presumably related to the Cu nanoparticle size, rather than the surface coverage, because TEM (Figure S6) shows ample free TiNT surface and because the DRIFTS spectra of TiNT and 6 Cu/TiNT under $CO_2$ are similar. Finally, the 0.3Cu/TiNT lacks large Cu nanoparticles (Figure S6), which precludes, by definition, the formation of SMSI overlayers. Therefore, the IR spectra of $CO_2$ adsorbed on the surfaces of $H_2$-treated TiNT, 0.3Cu/TiNT and 6Cu/TiNT are all similar and dominated by monodentate carbonate adsorbed at oxidized surfaces similar to those of the original TiNT. Under reaction conditions, these different surfaces (TiNT vs. Cu-O-Ti vs. nanoparticle Cu-TiNT) would lead to different active sites (e.g. O vacancies) at or near the interface, giving rise to the different apparent observed activation barriers.

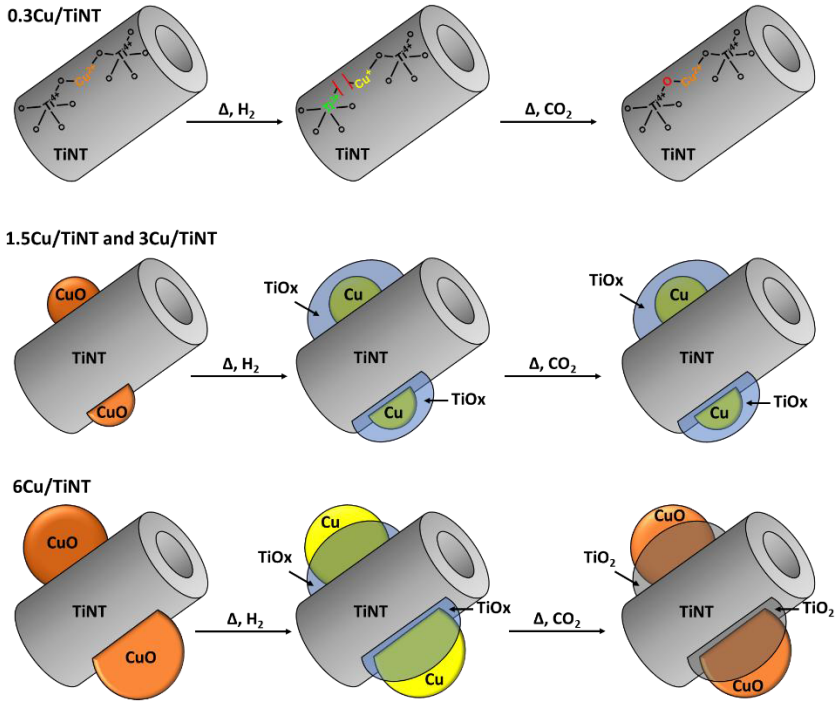


**Scheme 1.** Surface reconstruction on Cu/TiNT with different Cu loadings. On 0.3Cu/TiNT, oxygen vancancies are created during $H_2$ treatment and healed by $CO_2$ and elevated temperature See Figures 3 and 6 for DFT simulations of such sites. On 1.5Cu/TiNT and 3Cu/TiNT, SMSI overlayers with large numbers of potential RWGS active sites are formed on Cu during $H_2$ treatment but they prevent Cu from interacting with $CO_2$ and reoxidizing. On 6Cu/TiNT, overlayers only partially coat Cu during $H_2$ treatment and Cu remains accesible to $CO_2$.

After forming the surface carbonates in the procedures corresponding to Figure 5 and purging the cell with Ar, the samples were re-exposed to $H_2$ to follow the RWGS reaction and the evolution of new surface species. An example set of spectra for 0.3 Cu/TiNT under sequential Ar, $H_2$ and Ar flows are shown in **Figure 7**, along with the time dependent intensities at 1517 $cm^{-1}$ (monodentate carbonate) and 1616 $cm^{-1}$ (water). The monodentate carbonate species was rapidly depleted under $H_2$, while surface water was produced at roughly the same rate as the depletion of the monodentate carbonate species. Typical species formed during carbonate hydrogenation[61,62] such as formate (~1580 $cm^{-1}$)[63], and carboxylate (~1670 $cm^{-1}$)[64], were

not observed. As such, we can propose that the surface monodentate carbonate is the immediate precursor to CO formation.

This correlation between the depletion of surface carbonate and the formation of water was only observed on 0.3Cu/TiNT. On 1.5Cu/TiNT (**Figure 8**) and 3Cu/TiNT (Figure S8), both carbonate and water slowly decreased under $H_2$ and Ar flow. That is likely because the bidentate carbonate species on SMSI surface was converted to monodentate carbonate[29], which was readily depleted in $H_2$, and further reduction of the SMSI overlayers was unfavorable. Interestingly, the intensities of carbonate on both 6Cu/TiNT (Figure S9) and TiNT (Figure S10) remain nearly unchanged, while the increase of surface adsorbed water under $H_2$ is attributed to the reaction of $H_2$ with surface oxygen.

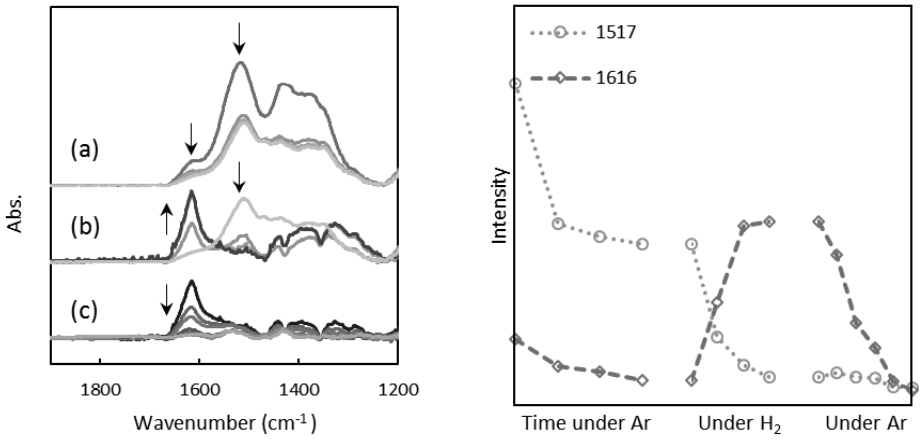


**Figure 7.** Left: IR spectra of $CO_2$ adsorbed 0.3Cu/TiNT under sequential flows of (a) Ar (30 min), (b) $H_2$ (5 min) and (c) Ar (30 min). Right: The plots of intensities at 1517 and 1616 $cm^{-1}$ versus time.

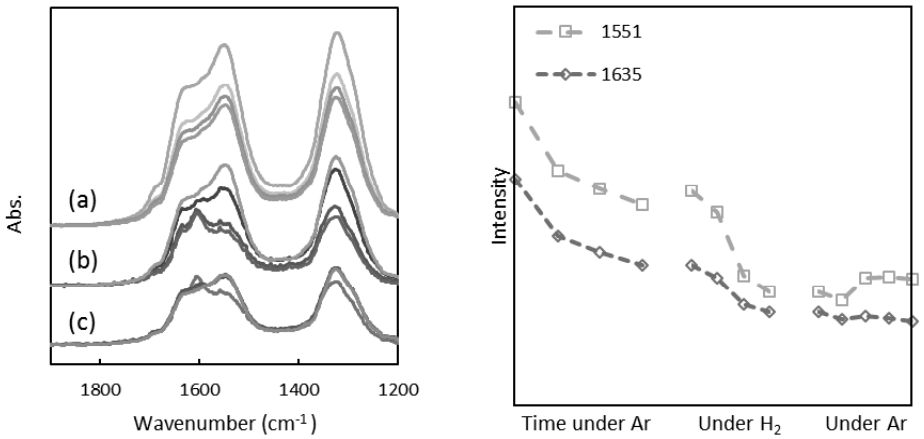


**Figure 8.** Left: IR spectra of $CO_2$ adsorbed 1.5Cu/TiNT under sequential flows of (a) Ar (30 min), (b) $H_2$ (5 min) and (c) Ar (30 min). Right: The plots of intensities at 1551 and 1635 $cm^{-1}$ versus time.

## Conclusion

It is generally accepted that surface reconstruction plays an important role in creating the active sites of a catalyst. Phenomena such as SMSI are well known in catalysis and extensively studied for supported metals such as Pt[65-67], Pd[68,69], and Au[70]. A SMSI-like overlayer was recently implicated in the catalytic activity of Rh for $CO_2$ hydrogenation[25]. In the present study, significant changes in apparent activation energy for RWGS were observed as the metal surface density changed for Cu/TiNT catalysts. Specifically, we propose that materials with exposed Cu and TiNT surfaces, either in 0.3Cu/TiNT or 6Cu/TiNT, create catalysts with lower energy barriers than on 1.5Cu/TiNT and 3Cu/TiNT, where Cu is inaccessible to the reactants as a result of SMSI. While unfortunately preventing formation of the lowest-barrier sites, the TiOx created by the SMSI does remain catalytically active. These sites have the same apparent barrier as those in the original TiNT, but appear to be far more numerous. Active sites like O vacancies are presumably rare on the bare titania surfaces, but it is known that thin oxide overlayers have different structures than do the bulk oxides. [71] The increase in activity for all Cu/TiNT samples vs. Cu/TiNP is also likely related to the creation of more O vacancies on the highly-strained and

preferentially anatase 001 surfaces of TiNT. [27-31] *In situ* UV-visible and IR spectroscopy show that such SMSI overlayers can form on top of Cu domains after exposure to $H_2$ at 300 °C. When $CO_2$ interacts with reduced 1.5Cu/TiNT and 3Cu/TiNT, where the metallic Cu surface is blocked by the SMSI overlayers, bidentate carbonate species are formed. However, when $CO_2$ interacts with the reduced 0.3Cu/TiNT, Cu assists $TiO_2$ in $CO_2$ activation, as supported by DFT calculations. The difference in the activation barriers between 0.3Cu/TiNT and 1.5Cu/TiNT or 3Cu/TiNT suggests an active site may be created at the Cu-O-Ti sites in 0.3Cu/TiNT. The altered actiation barriers indicate that Cu and TiNT surfaces are both involved in $CO_2$ activation over 6 Cu/TiNT. The exact mechanisms will require further investigation in all cases. This study provides insights for creating effective supported metal catalysts for $CO_2$ activation and conversion.

**Acknowledgements**

This research was funded by the National Science Foundation (CBET-1438721). The Department of Energy (DE-FG02-03ER15457) is acknowledged for support of S.L.N. and the CleanCat core facility (DRIFTS and TPR). The Institute for Sustainability and Energy at Northwestern is acknowledged for support of A.G. and for reactor construction. This work made use of the J.B. Cohen X-ray Diffraction Facility and the SPID facility at Northwestern University. These are supported by the MRSEC program of the National Science Foundation (DMR-1121262, DMR-1720139) and the Soft and Hybrid Nanotechnology Experimental (SHyNE) Resource (NSF NNCI-1542205). the International Institute for Nanotechnology (IIN), the Keck Foundation, and the State of Illinois. Metal analysis was performed at the Northwestern University Quantitative Bio-element Imaging Center. M.N. acknowledges support from Science

Foundation Ireland through the US-Ireland R&D Parntershop program, Grant number SFI/US/14/e2915, access to SFI funded computing resources at Tyndall Institute and the SFI/HEA funded Irish Centre for High End Computing, and support from the COST Action CM1104 "Reducible Metal Oxides, Structure and Function."

**References**

1. G. Centi, E.A. Quadrelli, S. Perathoner, Siglinda, Catalysis for $CO_2$ Conversion: A Key Technology for Rapid Introduction of Renewable Energy in the Value Chain of Chemical Industries. Energy Environ. Sci. 6 (2013) 1711-1731.
2. S. Saeidi, N.A.S Amin, M.R. Rahimpour, Hydrogenation of $CO_2$ to Value-Added Products—a Review and Potential Future Developments. Journal of $CO_2$ Utilization 5 (2014) 66-81.
3. M.S. Spencer, On the Activation Energies of the Forward and Reverse Water-Gas Shift Reaction. Catal. Lett. 32 (1995) 9-13.
4. D.S. Newsome, The Water-Gas Shift Reaction. Catal. Rev. 21 (2006) 275-318.
5. Y.A. Daza, J.N. Kuhn, $CO_2$ Conversion by Reverse Water Gas Shift Catalysis: Comparison of Catalysts, Mechanisms and Their Consequences for $CO_2$ Conversion to Liquid Fuels. RSC Advances 6 (2016) 49675-49691.
6. J. Graciani, et al., Highly Active Copper-Ceria and Copper-Ceria-Titania Catalysts for Methanol Synthesis from $CO_2$. Science 345 (2014) 546-550.
7. I. Toyoshima, G.A. Somorjai, Heats of Chemisorption of $O_2$, $H_2$, CO, $CO_2$, and $N_2$ on Polycrystalline and Single Crystal Transition Metal Surfaces. Catal. Rev. 19 (1979) 105-159.
8. C.C. Yang, Y.H. Yu, B. van der Linden, J.C. Wu, G. Mul, Artificial Photosynthesis over Crystalline $TiO_2$-Based Catalysts: Fact or Fiction? J. Am. Chem. Soc. 132 (2010), 8398-406.
9. H. Yamashita, Photocatalytic Reduction of $CO_2$ with $H_2O$ on $TiO_2$ and Cu/$TiO_2$ Catalysts. Res. Chem. Intermed 20 (1994) 815-823.
10. T. Tagawa, N. Nomura, M. Shimakage, S. Goto, Effect of Supports on Copper Catalysts for Methanol Synthesis from $CO_2$ + $H_2$. Res. Chem. Intermed. 21 (1995) 193-202.
11. S.I. In, D.D. Vaughn, R.E. Schaak, Hybrid CuO-$TiO_{2-x}N_x$ Hollow Nanocubes for Photocatalytic Conversion of $CO_2$ into Methane under Solar Irradiation. Angew. Chem. Int. Ed. 51 (2012) 3915-8.
12. K.K. Bando, K. Sayama, H. Kusama, K. Okabe, H. Arakawa, In-Situ Ft-Ir Study on $CO_2$ Hydrogenation over Cu Catalysts Supported on $SiO_2$, $Al_2O_3$, and $TiO_2$. Appl. Catal., A 165 (1997) 391-409.13. T.C. Schilke, I.A. Fisher, A.T. Bell, Influence of Titania on Zirconia Promoted Cu/$SiO_2$ Catalysts for Methanol Synthesis from CO/$H_2$ and $CO_2$/$H_2$. Catal. Lett. 54 (1998) 105-111.
14. M.C. Bradford, C.J. Michael, M. Albert Vannice, The Role of Metal–Support Interactions in $CO_2$ Reforming of $CH_4$. Catal. Today 50 (1999) 87-96.
15. T.C. Schilke, I.A. Fisher, A.T. Bell, In Situ Infrared Study of Methanol Synthesis from $CO_2$/H2on Titania and Zirconia Promoted Cu/$SiO_2$. J. Catal. 184 (1999) 144-156.
16. I.H. Tseng, W-C Chang, J.C.S. Wu, Photoreduction of $CO_2$ Using Sol–Gel Derived Titania and Titania-Supported Copper Catalysts. Appl. Catal., B 37 (2002) 37-48.
17. D. Shi, Y. Feng, S. Zhong, Photocatalytic Conversion of $CH_4$ and $CO_2$ to Oxygenated Compounds over Cu/CdS– $TiO_2$/$SiO_2$ Catalyst. Catal. Today 98 (2004) 505-509.

18. I.H. Tseng, J.C.S. Wu, H-Y Chou, Effects of Sol–Gel Procedures on the Photocatalysis of Cu/ $TiO_2$ in $CO_2$ Photoreduction. J. Catal. 221, (2004) 432-440.
19. N. Slamet; H. Nasution, E. Purnama, S. Kosela, J. Gunlazuardi, Photocatalytic Reduction of $CO_2$ on Copper-Doped Titania Catalysts Prepared by Improved-Impregnation Method. Catal. Commun. 6 (2005) 313-319.
20. B. Srinivas, B. Shubhamangala, K. Lalitha, P. Anil Kumar Reddy, V. Durga Kumari, M. Subrahmanyam, D.B.R. Machiraju, Photocatalytic Reduction of $CO_2$ over Cu-$TiO_2$/Molecular Sieve 5A Composite. Photochem. Photobiol. 87 (2011) 995-1001.
21. D. Liu, Y. Fernández, O. Ola, S. Mackintosh, M. Maroto-Valer, C.M.A. Parlett, A.F. Lee, F. Adam, J.C.S. Wu, On the Impact of Cu Dispersion on $CO_2$ Photoreduction over Cu/$TiO_2$. Catal. Commun. 25 (2012) 78-82.
22. L. Liu, F. Gao, H. Zhao, Y. Li, Tailoring Cu Valence and Oxygen Vacancy in Cu/$TiO_2$ Catalysts for Enhanced $CO_2$ Photoreduction Efficiency. Appl. Catal., B 134-135 (2013) 349-358.
23. S. Neatu, J.A. Macia-Agullo, P. Concepcion, G. Garcia, Gold-Copper Nanoalloys Supported on $TiO_2$ as Photocatalysts for $CO_2$ Reduction by Water. J. Am. Chem. Soc. 136 (2014) 15969-76.
24. G.A. Somorjai, Surface Reconstruction and Catalysis. *Annu. Rev. Phys. Chem. 45 (1994)* 21-751.
25. J.C. Matsubu, S. Zhang, L. DeRita, N.S. Marinkovic, J.G. Chen, G.W. Graham, X. Pan, P. Christopher, Adsorbate-Mediated Strong Metal–Support Interactions in Oxide-Supported Rh Catalysts. Nat. Chem. 9 (2017**)** 120-127.
26. J. Strunk, M.A. Bañares, I.E. Wachs, Vibrational Spectroscopy of Oxide Overlayers. Top. Catal. 60 (2017) 60, 1577-1617.
27. D. Finkelstein-Shapiro, C.Y.H. Tsai, S. Li, K.A. Gray, Synthesis of High-Energy Anatase Nanorods Via an Intermediate Nanotube Morphology. Chem. Phys. Lett. 546 (2012) 106-108.
28. K.C. Schwartzenberg, K.A. Gray, Nanostructured Titania: The Current and Future Promise of Titania Nanotubes. Cat. Sci. Tec. 2 (2012) 1617-1624.
29. W. Wu, K. Bhattacharyya, K.A. Gray, E. Weitz, Photoinduced Reactions of Surface-Bound Species on Titania Nanotubes and Platinized Titania Nanotubes: An in Situ FTIR Study. J. Phys. Chem. C 117 (2013) 20643-20655.
30. K. Bhattacharyya, A. Danon, B. K.Vijayan, K.A. Gray, P.C. Stair, E. Weitz, Role of the Surface Lewis Acid and Base Sites in the Adsorption of $CO_2$ on Titania Nanotubes and Platinized Titania Nanotubes: An in situ FT-IR Study. J. Phys. Chem. C 117 (2013) 12661-12678.
31. B. Vijayan, N.M. Dimitrijevic, T. Rajh, K.A. Gray, Effect of Calcination Temperature on the Photocatalytic Reduction and Oxidation Processes of Hydrothermally Synthesized Titania Nanotubes. J. Phys. Chem. C 114 (2010) 12994-13002.
32. S.L Nauert, F. Schax, C. Limberg, J.M. Notestein, Cyclohexane Oxidative Dehydrogenation over Copper Oxide Catalysts. J. Catal. 341(2016) 180-190.
33. G. Kresse, J. Hafner, J., *Ab initio* molecular-dynamics simulation of the liquid-metal-amorphous-semiconductor transition in germanium. Phys. Rev. B. 49 20 (1994) 14251-14269.
34. J. Furthmüller, J. Hafner, G. Kresse, Dimer reconstruction and electronic surface states on clean and hydrogenated diamond (100) surfaces. Phys. Rev. B.53 11 (1996) 7334-7351.
35. P.E. Blochl, Projector Augmented-Wave Method. Phys Rev B 50 24 (1994) 17953-17979.

36. G. Kresse, D. Joubert, From ultrasoft pseudopotentials to the projector augmented-wave method. Phys Rev B 59 3 (1999) 1758-1775.
37. J.P. Perdew, K. Burke, M. Ernzerhof, Generalized gradient approximation made simple. Phys. Rev. Lett. 77 18 (1996) 3865-3868.
38. V.I. Anisimov, J. Zaanen, O.K. Andersen, Band theory and Mott insulators: Hubbard U instead of Stoner I. Phys. Rev. B. 44 3 (1991) 943-954.
39. S.L. Dudarev, G.A. Botton, S.Y. Savrasov, C.J. Humphreys, A.P. Sutton, Electron-energy-loss spectra and the structural stability of nickel oxide: An LSDA+U study. Phys. Rev. B. 57 3 (1998) 1505-1509
40. X. Xue, W. Ji, Z, Mao, Zhu; H. Mao, Y. Wang, X.Wang, W. Ruan, B. Zhao, J.R. Lombardi, Raman Investigation of Nanosized $TiO_2$: Effect of Crystallite Size and Quantum Confinement. J. Phys. Chem. C 116 (2012) 8792-8797.
41. F.J. Xu, W.X. Ji. Z. Shen, S.W. Li, H.S. Tang, X.Ye, Z.D. Jia, Q.X. Xin, Raman Spectra of CuO Nanocrystals. Journal of Raman Spectroscopy 30 (1999) 413-415.
42. A. Kubacka, M.J. Muñoz-Batista, M. Fernández-García, S. Obregón, G Colón, Evolution of $H_2$ Photoproduction with Cu Content on Cuox- $TiO_2$ Composite Catalysts Prepared by a Microemulsion Method. Appl. Catal., B 163 (2015) 214-222.
43. H. Zhu, L. Dong, Y. Chen, Effect of Titania Structure on the Properties of Its Supported Copper Oxide Catalysts. J. Colloid Interface Sci. 357 (2011) 497-503.
44. G.C. Bond, S.N. Namijo, J.S. Wakeman, Thermal Analysis of Catalyst Precursors: Part 2. Influence of Support and Metal Precursor on the Reducibility of Copper Catalysts. J. Mol. Catal. 64 (1991) 305-319.
45. B. Xu, L. Dong, Y. Chen, Influence of Cuo Loading on Dispersion and Reduction Behavior of CuO/ $TiO_2$ (Anatase) System. J. Chem. Soc., Faraday Trans. 94 (1998) 1905-1909.
46. S.L. Nauert, A.S. Rosen, H. Kim, R.Q. Snurr, P.C. Stair, J.M. Notestein, Evidence for Copper Dimers in Low-Loaded CuOx/$SiO_2$ Catalysts for Cyclohexane Oxidative Dehydrogenation. ACS Catal. 8 (2018) 9775-9789.
47. J. Lee, Y.H. Lee, J.S. Choi, K.S. Park, K.S.Chang, M.Yoon, Hydrothermal Synthesis of Defective $TiO_2$ Nanoparticles for Long-Wavelength Visible Light-Photocatalytic Killing of Cancer Cells. RSC Advances 5 (2015) 99789-99796.
48. M. Mousavi-Kamazani, Z. Zarghami, R. Rahmatolahzadeh, M.Ramezani, Solvent-Free Synthesis of Cu-Cu2O Nanocomposites Via Green Thermal Decomposition Route Using Novel Precursor and Investigation of Its Photocatalytic Activity. Adv. Powder Technol. 28 (2017) 2078-2086.
49. A. Marimuthu, J. Zhang, S. Linic, Tuning Selectivity in Propylene Epoxidation by Plasmon Mediated Photo-Switching of Cu Oxidation State. Science 339 (2013) 1590-1593.
50. J. Nakamura,J.A. Rodriguez, C.T. Campbell, Does $CO_2$dissociatively Adsorb on Cu Surfaces? J. Phys.: Condens. Matter 1 (1989) SB149-SB160.
51. F. Muttaqien, Y. Hamamoto, K. Inagaki, Y. Morikawa, Yoshitada, Dissociative Adsorption of $CO_2$ on Flat, Stepped, and Kinked Cu Surfaces. J. Chem. Phys. 141 (2014) 034702.
52. B. Eren, R.S. Weatherup, N. Liakakos, G.A. Somorjai, M. Salmeron, Dissociative Carbon Dioxide Adsorption and Morphological Changes on Cu(100) and Cu(111) at Ambient Pressures. J. Am. Chem. Soc. 138 (2016) 8207-8211.
53. G. Busca, V. Lorenzelli, V., Infrared Spectroscopic Identification of Species Arising from Reactive Adsorption of Carbon Oxides on Metal Oxide Surfaces. Mater. Chem. 7 (1982) 89-126.

54. K.S. Finnie, D.J. Cassidy, J.R. Bartlett, J.L. Woolfrey, Ir Spectroscopy of Surface Water andHydroxyl Species on Nanocrystalline $TiO_2$ films. Langmuir 17 (2001) 816-820.
55. K. Tanaka, J.M. White, Characterization of Species Adsorbed on Oxidized and Reduced Anatase. J. Phys. Chem. 86 (1982) 4708-4714.
56. A.M. Turek, I.E. Wachs, E. DeCanio, Acidic Properties of Alumina-Supported Metal Oxide Catalysts: An Infrared Spectroscopy Study. J. Phys. Chem. 96 (1992) 5000-5007.
57. M. Takeuchi, L. Bertinetti, G. Martra, S. Coluccia, M. Anpo, States of $H_2O$ Adsorbed on Oxides: An Investigation by near and Mid Infrared Spectroscopy. *Appl. Catal., A 307 (2006)* 13-20.
58. J. Soria, J. Sanz, I. Sobrados, J.M. Coronado, A.J. Maira, M.D. Hernández-Alonso, F. Fresno, Ftir and Nmr Study of the Adsorbed Water on Nanocrystalline Anatase. J. Phys. Chem. C 111 (2007) 10590-10596.
59. S.J. Tauster, S.C. Fung, R.T.K. Baker, J.A. Horsley, Strong Interactions in Supported-Metal Catalysts. Science 211 (1981) 1121-1125.
60. S. Zhang, P.N. Plessow, J.J. Willis, S. Dai, M. Xu, G.W. Graham, M. Cargnello, F. Abild-Pedersen, X. Pan, Dynamical Observation and Detailed Description of Catalysts under Strong Metal–Support Interaction. Nano Lett. 16 (2016) 4528-4534.
61. L.C. Grabow, M. Mavrikakis, Mechanism of Methanol Synthesis on Cu through $CO_2$ and CO Hydrogenation. ACS Catal. 1 (2011) 365-384.
62. F. Studt, et al., The Mechanism of CO and $CO_2$ Hydrogenation to Methanol over Cu-Based Catalysts. ChemCatChem 7 (2015) 1105-1111.
63. D.H. Gibson, Carbon Dioxide Coordination Chemistry: Metal Complexes and Surface-Bound Species. What Relationships? Coord. Chem. Rev. 185-186 (1999) 335-355.
64. W.Su, J. Zhang, Z. Feng, T. Chen, P. Ying, C. Li, Surface Phases of $TiO_2$ Nanoparticles Studied by Uv Raman Spectroscopy and Ft-Ir Spectroscopy. J. Phys. Chem. C 112 (2008) 7710-7716.
65. S.C. Fung, Xps Studies of Strong Metal-Support Interactions (SMSI)—$PtTiO_2$. J. Catal. 76 (1982) 225-230.
66. A.K. Datye, D.S. Kalakkad, M.H. Yao, D.J. Smith, Comparison of Metal-Support Interactions in Pt/ $TiO_2$ and Pt/$CeO_2$. J. Catal. 155 (1995) 148-153.
67. O. Dulub, W. Hebenstreit, U. Diebold, Imaging Cluster Surfaces with Atomic Resolution: The Strong Metal-Support Interaction State of Pt Supported on $TiO_2$ (110). Phys. Rev. Lett. 84 (2000) 3646-3649.
68. M.A. Vannice, S.Y. Wang, S.H. Moon, The Effect of Smsi (Strong Metal-Support Interaction) Behavior on Co Adsorption and Hydrogenation on Pd Catalysts: I. Ir Spectra of Adsorbed Co Prior to and During Reaction Conditions. J. Catal. 71 (1981) 152-166.
69. M.S.. Kim, S.H. Chung, C.J. Yoo, M.S. Lee, I.H. Cho, D.W. Lee, K.Y Lee, Catalytic Reduction of Nitrate in Water over Pd–Cu/ $TiO_2$ Catalyst: Effect of the Strong Metal-Support Interaction (SMSI) on the Catalytic Activity. Appl. Catal., B 142-143 (2013) 354-361.
70. H. Tang, et al., Classical Strong Metal–Support Interactions between Gold Nanoparticles and Titanium Dioxide. Science Advances 3 (2017).
71. H.V. Thang, S. Tosoni, G. Pacchioni, Evidence of Charge Transfer to Atomic and Molecular Adsorbates on ZnO/X(111) (X = Cu, Ag, Au) Ultrathin Films. Relevance for Cu/ZnO Catalysts. ACS Catal. 8 (2018) 4110-4119.

*Graphical Abstract

# Role of surface reconstruction on $Cu/TiO_2$ nanotubes for $CO_2$ conversion

Chao Liu,[1] Scott L. Nauert,[2] Marco A. Alsina,[1] Dingdi Wang,[3] Alexander Grant,[2] Kai He,[4] Eric Weitz,[3,*] Michael Nolan,[5] Kimberly A. Gray,[1,*] Justin M. Notestein,[2,*]

[1]Department of Civil and Environmental Engineering, [2]Department of Chemical and Biological Engineering, [3]Department of Chemistry, [4]Department of Materials Science and Engineering, Northwestern University, Evanston, Illinois 60208, United States
[5]Tyndall National Institute, University College Cork, Lee Maltings, Cork, Ireland
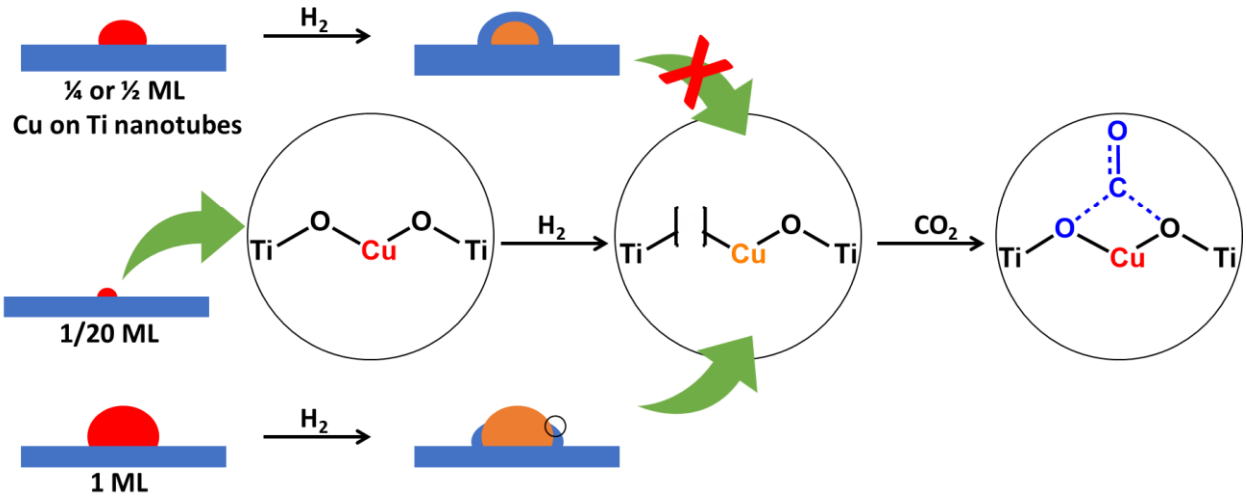
## Graphical Abstract